Dalton Transactions

ROYAL SOCIETY OF CHEMISTRY

PAPER

View Article Online
View Journal | View Issue

Cite this: *Dalton Trans.*, 2025, **54**, 17851

Electron-withdrawing groups as property tuners in functionalized terpyridine-based ligands in Eu(III) and Tb(III) complexes

Oksana Fizer,[a] Sina Chiniforoush,[b] Thomas J. Summers,[b] Mohammad Zafar Abbas,[a] David C. Cantu [b] and Ana de Bettencourt-Dias *[a]

Three terpyridine derivatives with electron-withdrawing groups in the *ortho*-position of terpyridine, $-NO_2$ (terpyNO_2), −CHO (terpyCHO) and −Br (terpyBr), were isolated and the influence of these substituents on the chemical and photophysical characteristics of the corresponding Eu(III), Tb(III) and Dy(III) complexes was assessed and compared with the complexes with unsubstituted terpyridine. A direct correlation between the complex stability constants and the second pK_{a_2} values of the free ligands was found. Emission quantum yields indicate moderate ability to sensitize the metal-centered emission. Judd–Ofelt intensity parameters and energy transfer rates were calculated for all complexes. A direct correlation was found between the forward energy transfer rates and the sensitization efficiency for the Eu(III) complexes. For the Tb(III)-based complexes back-energy transfer from the metal ion to the ligands' triplet level dominates. At 298 K, the Eu(III) complexes displayed emission lifetimes in the range 1.49–1.68 ms, while for the Tb(III) complexes the lifetimes were in the range 0.71–1.17 ms. The lifetimes of all the complexes could be fit with a single exponential at this temperature. However, at 77 K, double-exponential decay was observed. Nuclear magnetic resonance (NMR) analysis and density functional theory (DFT) calculations, modeled on the Eu(III)-terpyNO_2 complex are consistent with decomplexation and subsequent rotation of one of the ligand's pyridine rings, which lead to the observed two species in frozen solution.

Received 8th October 2025,
Accepted 13th November 2025

DOI: 10.1039/d5dt02417j

rsc.li/dalton

Introduction

The interest in luminescent lanthanide (Ln(III)) ion complexes is dictated by the metal ions' unique optical properties,[1] which make them useful for a variety of functional materials,[2–5] such as OLEDs and lighting,[6–10] biosensors,[11–15] and chemical sensors.[16] Moreover, Ln(III) ion complexes have interesting metal-based magnetic properties, and are explored as single-molecule magnets[17–19] and as magnetic resonance imaging contrast agents; they have also garnered interest as therapeutic agents in chemotherapy.[20,21] While the magnetic and optical properties are metal-based, variation of the ligand structure enables fine-tuning the properties of the complexes depending on the application.[22–27]

The molecular design of ligands for lanthanide-based complexes is a powerful approach to developing new materials and compounds with predefined and tuned properties. While searching for design criteria for enhancing magnetic hysteresis of Dy(III) single-molecule magnets (SMMs), Yu *et al.* found that replacing the ligand butoxide with a more hindered phenylethanolate in $[Dy(OR)_2(py)_5][BPh_4]$ leads to reduced quantum tunnelling at low temperatures and thus higher temperature of magnetic hysteresis.[28] Corner *et al.* showed that adding one halobenzene PhX (X = F, Cl, Br) as additional equatorial ligand in a dysprosocenium-based SMM reduces the magnetic hysteresis temperature compared to the unsubstituted compound, due to an increase in the Orbach and two-phonon relaxation mechanisms, which correlate with the presence of the halide atoms bound to the metal ion.[29] In the presence of two equatorial halobenzenes, a significant bending of the Cp*···Dy···Cp* moiety occurs, which promotes relaxation mechanisms.[30] Building on the dysprosocenium architecture, Ullah *et al.* showed that it was possible to tune the blocking temperature of dysprosocenium-type SMMs by varying the cyclopentadienyl ring substituents.[31] Photoluminescence can be modulated as well through ligand substitution, as demonstrated by Romanova *et al.*, who showed the use of the substituted 2-phenoxy-1,10-phenanthroline sensitizer for improved Eu(III) luminescence.[32]

In the search for efficient sensitizers for Ln(III) ion emission, and unique modes of coordination for Ln(III) ion complexes, our group isolated several complexes with ligands bearing a $-NO_2$ functional group, including a terpyridine functionalized at the *ortho*-position, terpyNO_2. We found that the

[a]*Department of Chemistry, University of Nevada, Reno, 1664 N. Virginia Street, Reno, NV 89557, USA. E-mail: abd@unr.edu*
[b]*Department of Chemical and Materials Engineering, University of Nevada, Reno, 1664 N. Virginia Street, Reno, NV 89557, USA*

nitro moiety coordinated to the metal ion through one of its oxygen atoms and that the ligand sensitized metal-centred emission for both Eu(III) and Tb(III), yet yielded relatively weak luminescence.[33]

With the purpose of investigating the influence of other electron-withdrawing groups (EWGs) in the *ortho*-position of terpyridine ligands on the spectroscopic properties of their complexes with Eu(III), Tb(III) and Dy(III) ions, we isolated terpyBr, terpyCHO and compared the photophysical properties of their complexes with the complexes of terpyNO_2 and the unsubstituted terpy. Our focus on these systems was made due to versatility of terpyridine heterocyclic system in coordination chemistry of Ln(III),[34–36] and the ease of functionalization.[37–39] While the selected EWGs should decrease the electron density on the terpyridine system and thus decrease its complexation ability, their localization at the *ortho*-position should allow to form an additional coordination bond to the central Ln(III) ion, thus increasing complex stability and decreasing the ability of solvent molecules to coordinate to the metal ion, which frequently results in vibrational quenching of the emission.

Experimental

General information

Starting materials purchased from commercial sources were used as received without further purification, unless otherwise indicated, and the solvents were dried by standard methods. All lanthanide salts were dried under reduced pressure at 60 °C for 12 h. Stock solutions of the Ln(III) (Ln = Eu(III), Gd (III), Tb(III) and Dy(III)) nitrate salts were prepared in spectroscopic grade acetonitrile. Concentration of the Ln(III) salt solutions was determined by complexometric titrations with EDTA (0.01 M) using xylenol orange as indicator.[40] Unless otherwise indicated, all reactions were done under inert atmosphere.

NMR spectra were recorded on Varian 400 and 500 MHz spectrometers, and the chemical shifts were reported (ppm) against tetramethylsilane (TMS, 0.00 ppm) as the reference.

Mass spectra were recorded using an Agilent Technologies 6230 TOF LC/MS system with an electrospray ionization source.

Spectroscopic characterization

Absorption data were collected on a Perkin Elmer Lambda 35 spectrometer equipped with deuterium and tungsten halogen lamps and a concave grating with 105 lines per mm. Spectra were collected using a scan speed of 480 nm min^{-1} in the range 190–700 nm with a photodiode detector. All spectra were background corrected using solvent as the blank.

The emission and excitation spectra of the complexes were recorded on a Perkin Elmer LS-55 spectrometer equipped with a 450 W xenon discharge lamp at 298 and 77 K. All spectra were collected in the 200–800 nm range with a maximum scan speed of 250 nm min^{-1}. Emission lifetimes were measured on the same instrument using the Short Phosphorescence Decay software package.

Standards used for emission quantum yield measurements were $Cs_3[Eu(dpa)_3]$ (ϕ_{std} = 24%, 7.5 × 10^{-5} M in TRIS/HCl buffer (0.1 M, pH ~ 7.4) and $Cs_3[Tb(dpa)_3]$ in TRIS/HCl buffer (ϕ_{std} = 22%, $A_{279} \approx 0.18$, 6.5 × 10^{-5} M)[41] The excitation wavelength for the standards was 279 nm, while for the samples the excitation wavelength was 335 nm. The concentration of the samples was adjusted to have an absorption value $A < 0.10$. The quantum yield of the samples was determined by the dilution method using eqn (1), which accounts for the need to use of different excitation wavelengths of sample (x) and standard (std).

$$\phi_x^L = \phi_{std} \times \frac{Grad_x}{Grad_{std}} \times \left(\frac{n_x}{n_{std}}\right)^2 \times \frac{I_{std}}{I_x} \quad (1)$$

Grad is the slope of the plot of the integrated emission as a function of absorbance, n is the refractive index of the solvent, I is the intensity of the excitation source at the excitation wavelength and ϕ is the quantum yield.

The intrinsic quantum yield ϕ_{Ln}^{Ln} was determined using eqn (2).[42]

$$\phi_{Ln}^{Ln} = \frac{k_{rad}}{k_{tot}} = \frac{\tau_{exp}}{\tau_{rad}} \quad (2)$$

k_{tot} is the total emission rate ($k_{tot} = k_{rad} + k_{nrad} = 1/\tau_{exp}$), k_{rad} is the radiative rate constant, k_{nrad} is the non-radiative rate constant and τ_{exp} is the observed excited state lifetime. In the case of the Eu(III) complexes, k_{rad} can be determined using eqn (3).[42–44]

$$k_{rad} = \frac{1}{\tau_{rad}} = A_{MD,0} \times n^3 \times \frac{I_{tot}}{I_{MD}} \quad (3)$$

I_{tot} and I_{MD} are the total integrated emission spectrum and integrated intensity of the magnetic dipole-allowed $^5D_0 \rightarrow {}^7F_1$ transition of the Eu(III) ion, respectively, and $A_{MD,0}$ is the Einstein coefficient of spontaneous emission in vacuum (14.65 s^{-1}).

Due to our inability to measure the absorption spectra of the f–f transitions for the Tb(III) complexes and thus determine τ_{rad} experimentally,[42–44] its value was taken as 4 ms, as proposed by Klink *et al.*[45]

The sensitization efficiency (η_{sens}) was determined using eqn (4).[42,43]

$$\eta_{sens} = \frac{\phi_{Ln}^L}{\phi_{Ln}^{Ln}} \quad (4)$$

Unless otherwise indicated, all data were collected at 25.0 ± 0.1 °C and are the average of at least three independent measurements.

Synthesis of compounds

Synthesis of [2,2′:6′,2″-terpyridine]-6-carbaldehyde (terpyCHO).[46,47] Following a modified literature procedure, 6-bromo-2,2′-bipyridine (0.971 g, 4.13 mmol, 1.0 eq.),[48] 2-(1,3-

dioxolan-2-yl)-6-(tributylstannyl)pyridine (1.99 g, 4.54 mmol, 1.1 eq.)[49] and $Pd(PPh_3)_4$ (0.286 g, 0.25 mmol, 0.06 eq.) were stirred to reflux in dry toluene (30 ml) for 72 h. The solvent was removed under reduced pressure, 20 ml 4 M HCl was added, and the reaction mixture was stirred overnight at 60 °C. After cooling to room temperature, the mixture was neutralized with 2 M $NaHCO_3$. The suspension was extracted with $CHCl_3$ (3 × 30 ml), the organic phase separated, washed with water (3 × 30 ml), and brine (1 × 40 ml) and dried over magnesium sulphate. The isolated solid was purified by flash chromatography (ethylacetate : hexanes 1 : 2) to give the desired product in 12% yield (95 mg, 0.36 mmol).

^{1}H-NMR (500 MHz, $CDCl_3$) δ 7.32–7.26 (m, 1H), 7.81 (td, J = 7.7, 1.8 Hz, 1H), 8.01–7.91 (m, 3H), 8.45 (d, J = 7.8 Hz, 1H), 8.55 (d, J = 7.7 Hz, 2H), 8.66 (d, J = 4.8 Hz, 1H), 8.81 (d, J = 7.6 Hz, 1H), 10.13 (s, 1H) ppm (Fig. S1).

^{13}C-NMR (126 MHz, $CDCl_3$) δ 193.76, 156.78, 156.00, 155.61, 154.21, 152.34, 149.25, 138.10, 137.86, 136.89, 125.21, 123.91, 121.64, 121.44, 121.19, 121.13 ppm (Fig. S3).

ESI-MS (Fig. S12): terpyCHO. ESI-MS: [terpyCHO + H_2O]; m/z: 279.101 (calc), 279.088 (exp).

Synthesis of 6-bromo-2,2′;6′,2″-terpyridine (terpyBr).[50] Following a modified literature procedure, to a solution of 2,6-dibromopyridine (2.0 g, 4.5 mmol) and $Pd(PPh_3)_4$ (0.26 g, 0.225 mmol) in dry toluene, 6-(tributylstannyl)-2,2′-bipyridine (1.006 g, 4.5 mmol) was added and the mixture was heated to reflux overnight. The reaction mixture was cooled, diluted with water, mixed with a concentrated aqueous solution of caesium fluoride (3.3 g, 22.2 mmol) and stirred for 30 min at room temperature. The mixture was filtered through a Celite pad and extracted with toluene (3 × 30 ml) and the combined organic layer was dried over magnesium sulfate, filtered and the solvent removed under reduced pressure. The product was obtained as an off-white solid in 10% yield (126 mg, 0.40 mmol) after flash column chromatography with hexane : ethylacetate (3 : 1) as the eluent.

^{1}H-NMR (500 MHz, $CDCl_3$): δ 8.71 (d, J = 5.2 Hz, 1H), 8.58 (d, J = 7.9 Hz, 2H), 8.49–8.43 (m, 2H), 7.96 (t, J = 7.7 Hz, 1H), 7.86 (td, J = 7.7, 1.8 Hz, 1H), 7.71 (t, J = 7.7 Hz, 1H), 7.51 (d, J = 7.8 Hz, 1H), 7.37–7.31 (m, 1H) ppm (Fig. S2).

^{13}C-NMR (126 MHz, $CDCl_3$): δ 157.44, 156.02, 155.47, 149.20, 141.58, 139.14, 138.01, 136.86, 128.00, 123.86, 121.58, 121.41, 121.12, 119.77 ppm (Fig. S4).

ESI-MS (Fig. S8): terpyBr. ESI-MS: [terpyBr] + m/z: 312.014 (calc), 312.012 (exp).

Synthesis of 6-nitro-2,2′;6′,2″-terpyridine (terpyNO$_2$).[33] Following a literature procedure, 6-tributylstannyl-2,2′-bipyridine (1.0 g, 2.25 mmol) and 2-bromo-6-nitropyridine (0.50 g, 2.47 mmol) were mixed with 1 mol% $Pd(PPh_3)_4$ and LiCl (0.24 g, 5.6 mmol) and toluene were added. The mixture was heated to 110 °C overnight. The solvent was removed under reduced pressure and the reaction mixture purified by flash chromatography with hexane : ethylacetate (2 : 1) as eluent to afford a brown solid, which was washed with a small volume of acetonitrile to give the desired product as a white solid. Yield: 0.056 g (0.2 mmol, 9%).

^{1}H-NMR (500 MHz, $CDCl_3$): δ 7.34–7.30 (m, 1H), 7.86–7.82 (m, 1H), 7.97 (t, J = 7.8 Hz, 1H), 8.12 (t, J = 7.8 Hz, 1H), 8.20 (d, J = 7.8 Hz, 1H), 8.47 (d, J = 7.8 Hz, 1H), 8.53 (t, J = 7.8 Hz, 2H), 8.71–8.67 (m, 1H), 9.00–8.97 (m, 1H) ppm.

Synthesis of metal complexes

Equimolar solutions of terpyR (R = H, NO_2, Br, CHO) and the $Ln(NO_3)_3$ (Ln = Eu, Tb, Dy, and Gd) were refluxed for 24 h in acetonitrile. Each solution was filtered, and the solvent removed under reduced pressure. The obtained solid was washed with chloroform and dried under reduced pressure to afford the corresponding metal complexes in 80–86% yield. No yield is indicated when the complexes were not isolated, and the solutions were used as is for spectroscopy.

Eu-terpy. ESI-MS (Fig. S5): $[Eu(terpy)(NO_3)_2(CH_3CN)]^+$; m/z: 509.991 (calc), 509.996 (exp).

Tb-terpy. ESI-MS (Fig. S6): $[Tb(terpy)_2(NO_3)_2]^+$; m/z: 749.092 (calc), 749.094 (exp).

Dy-terpy. ESI-MS (Fig. S7): $[Dy(terpy)_2(NO_3)_2]^+$; m/z: 754.091 (calc), 754.101 (exp).

Eu-terpyCHO. Yield: 82%. ESI-MS (Fig. S13): $[Eu(terpyCHO)(NO_3)_2]^+$; m/z: 536.987 (calc), 536.973 (exp).

Tb-terpyCHO. Yield: 85%. ESI-MS (Fig. S14): $[Tb(terpyCHO)(CH_3CN)(NO_3)_2]^+$; m/z: 585.018 (calc), 584.995 (exp).

Dy-terpyCHO. Yield: 80%. ESI-MS (Fig. S15): $[Dy(terpyCHO)(CH_3CN)(NO_3)_2]^+$; m/z: 590.022 (calc), 590.012 (exp).

Eu-terpyNO$_2$. ESI-MS (Fig. S16): $[Eu(terpyNO_2)_2(NO_3)_2]^+$; m/z: 835.056 (calc), 835.061 (exp).

Tb-terpyNO$_2$. ESI-MS (Fig. S17): $[Tb(terpyNO_2)(NO_3)_2]^+$; m/z: 560.981 (calc), 560.986 (exp).

Dy-terpyNO$_2$. ESI-MS (Fig. S18): $[Dy(terpyNO_2)(NO_3)_2]^+$; m/z: 565.981 (calc), 565.982 (exp).

Eu-terpyBr. ESI-MS (Fig. S9): $[Eu(terpyBr)(NO_3)_2(CH_3CN)(H_2O)]^+$; m/z: 646.938(calc), 647.055 (exp).

Tb-terpyBr. ESI-MS (Fig. S10): $[Tb(terpyBr)_2(NO_3)_3]^+$; m/z: 969.908 (calc), 969.902 (exp).

Dy-terpyBr. ESI-MS (Fig. S11): $[Dy(terpyBr)(NO_3)_2]^+$; m/z: 598.907 (calc), 598.907 (exp).

Computational methods

Molecular geometries were optimized using the M06 functional.[51] For Eu, effective core potentials and the corresponding basis set (Stuttgart RSC Segmented + ECP)[52] were used, and the CC-PVTZ [53] basis set was used for the rest of the atoms. The thermal contribution to the Gibbs free energy was computed using vibrational frequencies obtained from frequency calculations.

To compute the energies of the optimized structures, the M06 functional was used in combination with the relativistic DKH-def2-TZVPP[54] basis set for non-metal atoms and SARC-DKH-TZVP for the Eu atom.[54–56] The relativistic Hamiltonian DKH2 was utilized during the calculations.[57] The solvent effect of the acetonitrile medium was modeled with the conductor-like polarizable continuum (CPCM) model in geometry optimizations and single point calculations.[58]

Solvent molecules were explicitly included in cases where their coordination was expected.

ChemAxon[59] online program was used for the prediction of pK_a values of the terpyR ligands. LUMPAC[60–62] was used to obtain the experimental and theoretical Judd–Ofelt parameters and energy transfer rates for the Eu-based complexes. Quantum chemical calculations needed for the LUMPAC algorithm were performed with RM1-Sparkle[59,60] and ZINDO/S levels of theory using MOPAC2016 [63] and ORCA,[64] respectively. Judd–Ofelt parameters and energy transfer rates for the complexes were obtained with JOYSpectra.[65]

The distortion parameter δ of the central polyhedron from the ideal polyhedron in RM1-Sparkle-optimized Ln-complexes was calculated with the Polynator program.[66] Complex stoichiometry in solution and corresponding stability constants were obtained from UV-VIS spectrophotometric titrations and estimated using the SupraFit software.[67]

Results and discussion

Complex formation and stability

Previous work by us[33,47] and others[68–78] showed that the terpyridine scaffold can bind Ln(III) ions and sensitize their luminescence. Moreover, its ease of functionalization provides opportunities to tune electronic and structural properties of the resulting metal complexes. In this work, we focused on three known terpy-based compounds with EWG groups, namely, 6 nitro-2,2′;6′,2″-terpyridine (terpyNO$_2$),[33] 6-bromo-2,2′;6′,2″ terpyridine (terpyBr),[50] and [2,2′:6′,2″]-terpyridine-]-6-carbaldehyde (terpyCHO).[46] terpyNO$_2$ was studied by our group and showed its ability to function as a tetradentate ligand and as a sensitizer in Eu(III) and Tb(III) complexes.[33,39] terpyCHO and terpyBr were intermediates in the synthesis of other terpy-based compounds, namely in the synthesis of oligopyridylimines[49] and of a ruthenium complex with a terpy-substituted porphyrin,[79] respectively. terpyBr was used to add the terpy moiety during the synthesis of polypyridyl-containing ligands[80,81] The vibrational energy features of terpyCHO were explored *via* two-dimensional infrared spectroscopy.[47] Despite a general interest in terpyridine-based ligands to sensitize Ln(III)-centred emission,[82–84] neither terpyCHO nor terpyBr had been studied in this context. This could stem from the known lability of lanthanide complexes with the terpyridine ligand (*vide infra*).

Nine complexes (Fig. 1) were isolated with these three functionalized terpyridine-based ligands with the nitrate salts of Eu(III), Tb(III), and Dy(III) in acetonitrile. We also synthesized the known terpyridine (terpy) complexes[85] of the same metal ions for comparison purposes. All complexes showed 1 : 1 stoichiometry (Fig. S19 and S30) with stability constants (Table 1) that decreased in the order terpy > terpyCHO > terpyBr > terpyNO$_2$. While the stability constants of the Gd(III) complexes were not determined, they were prepared as well, to determine singlet and triplet state energies (*vide infra*).

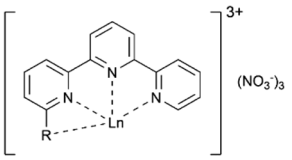

Ln-terpyR
Ln = Eu(III), Tb(III), Dy(III)
R = H, CHO, NO_2, Br

Fig. 1 Complexes studied here.

Table 1 Experimentally determined stability constants (log K) for the [Ln(terpyR)]$^{3+}$ (R = H, NO_2, CHO, Br; Ln(III) = Eu(III), Tb(III), Dy(III)) complexes in acetonitrile and ionic radii (r_{ion})

Ln (III)	r_{ion} [86] [Å]	log K terpy	terpyNO$_2$	terpyBr	terpyCHO
Eu	1.120	8.1 ± 0.2, 7.9 (ref. 77)	5.2 ± 0.4	5.5 ± 0.1	6.6 ± 0.1
Tb	1.095	7.9 ± 0.4	5.4 ± 0.5	5.5 ± 0.2	6.4 ± 0.1
Dy	1.083	7.9 ± 0.3	5.2 ± 0.5	5.4 ± 0.1	6.8 ± 0.4

The log K values of the substituted terpyridines, in the range 5.24–6.84, are smaller than the ones obtained for terpy, despite the possibility of tetradentate coordination. For the latter, the obtained value log K of 8.1 is in line with the reported value of 7.9;[77] the small difference is likely due to the different experimental conditions used, namely the 3 : 1 stoichiometry of the terpy complexes and our use of nitrate counter-ions, that are reported to successfully compete in acetonitrile for binding to the metal ion.[26] We do not observe statistically significant differences between stabilities of complexes of the same ligand with different metal ions, consistent with the similar sizes of the ions. Of the three terpyR ligands, terpyCHO binds Ln(III) most strongly.

To unravel the observed trend in log K, we studied the protonation of the ligands and found that the protonation of the outer unsubstituted pyridine ring appears most favourable (Table 2). For terpy, the calculated value of 4.46 compares well with the reported value of 4.54.[87] In the case of the substituted

Table 2 Protonation constants of the terpyR ligands, electronegativity (χ) of the R-groups

R=	–H	–NO_2	–Br	–CHO
pK_{a_1}	4.46 (ring 3), 4.54 (ref. 87)	4.17 (ring 3)	4.17 (ring 3)	4.17 (ring 3)
pK_{a_2}	3.85 (ring 1), 3.57 (ref. 87)	0.22 (ring 2)	0.37 (ring 2)	1.67 (ring 1)
pK_{a_3}	n.a.[a] (ring 2)	n.a.[a] (ring 1)	n.a.[a] (ring 1)	−1.70 (ring 2)
χ (ref. 88)	1.71	3.91	2.94	2.61

[a] n.a. – calculation did not converge.

terpyridines, the calculated pK_{a_1} of 4.17 indicates that the R-substituent has negligible influence on the electronics of this ring. The second protonation step is more complex; in the case of terpy, it occurs on the other outer pyridine ring and the calculated value of 3.85 agrees well with the reported value of 3.57.[87] In the case of the bromo- and nitro-substituted ligands, the protonation occurs on the middle pyridine ring, with pK_{a_2} values of 0.37 and 0.22, respectively. In the case of terpyCHO, the pK_{a_2} of 1.67 corresponds to the protonation of the first, functionalized pyridine ring. We attribute this difference to the high electron-withdrawing effect of the Br- and NO_2-groups, which decrease the basicity of the neighbouring ring, and absence of protonation of the substituted ring. Despite this discrepancy, pK_{a_2} correlates well with log K (Fig. 2a). Similar arguments involving substituent electronegativity χ, following the scale developed by Dailey and Shoolery,[88] indicate that χ decreases for NO_2 > Br > CHO > H and tracks with log K (Fig. 2b).

Photophysical characterization

All substituted terpyR sensitized the emission of Eu(III), Tb(III) and Dy(III). Absorption, emission, and excitation spectra of acetonitrile solutions of the Eu(III)-based complexes are shown in Fig. 3, those of the Tb(III)-based complexes are in Fig. S31–S34 and those of the Dy(III)-based complexes are in Fig. S35–S37. The analogous spectra at 77 K are shown in Fig. S38–S48. The absorption was most red-shifted for the complexes with terpyCHO and most blue-shifted for the complexes with terpyBr. As all complexes absorbed around 335 nm, the complexes were excited at this wavelength in all cases. The corresponding emission spectra display peaks at 588, 595, 617, 656, and 685 nm characteristic of the Eu(III)-centred $^5D_0 \rightarrow {}^7F_J$ (J = 0, 1, 2, 3, 4) transitions, 490, 545, 583, 623 nm, $^5D_4 \rightarrow {}^7F_J$ (J = 6, 5, 4, 3) for the Tb(III)-centred and 482, 575, 663 nm, $^4F_{9/2} \rightarrow {}^6H_J$ (J = 15/2, 13/2, 11/2) for the Dy(III)-centred transitions.

Table 3 summarizes the photophysical data for the Eu(III) and Tb(III) complexes. The ^{1}S and ^{3}T excited-state energies for terpy, determined in this work, were 27 950 and 22 200 cm^{-1}, respectively, higher than the reported values of 26 178 and 20 041 cm^{-1}.[77] This difference is likely due to the slightly different complex used by the authors, namely 3 : 1 $[La(terpy)_3]ClO_4$,[77] as well as slight differences in the deconvolution of the experimental spectra. For terpyNO_2, terpyBr and terpyCHO ^{1}S energies were 27 900, 27 330 and 28 000 cm^{-1}, respectively, and ^{3}T energies were 22 200, 22 860, 21 740, and 21 880 cm^{-1}, respectively. All ^{1}S–^{3}T gaps are larger than 5000 cm^{-1}, which facilitates the intersystem crossing.[90] The ^{3}T states are higher in energy than the emissive states of both Eu(III) and Tb(III), consistent with their ability to sensitize the metal-centered emission. The sensitized emission efficiency ϕ^{L}_{Ln} of the Eu(III) complexes is highest for terpyBr and terpyCHO, which have ^{3}T-f* gaps of 4510 and 4650 cm^{-1}, respectively, and lowest for terpy and terpyNO_2, which have the largest ^{3}T-f* gaps, at 4970 and 5630 cm^{-1}, respectively. For all Eu(III) complexes we observed that the sensitization efficiency η_{sens} correlates inversely with the energy of the triplet state (Fig. 4a).

Tb(III), with its $^5D_4$ emissive level at 20 500 cm^{-1}, is most efficiently sensitized by terpyBr, for which the ^{3}T-f* gap is 1240 cm^{-1}. This is, surprisingly, the narrowest gap, and should yield a substantial degree of back-energy transfer.[91] In fact, the

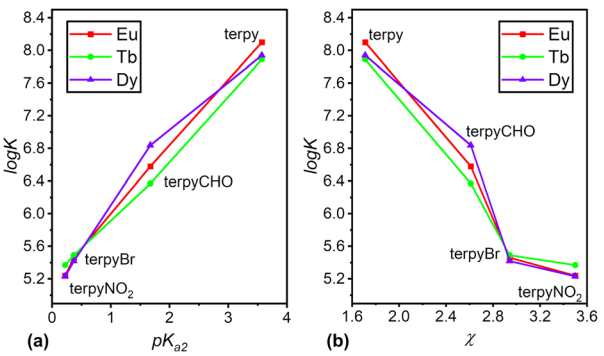

Fig. 2 Correlation of log K of the Ln(III) (Ln = Eu, Tb, Dy) complexes with (a) pK_{a_2}, and (b) electronegativity χ of the ligands. The connecting lines are visual aids.

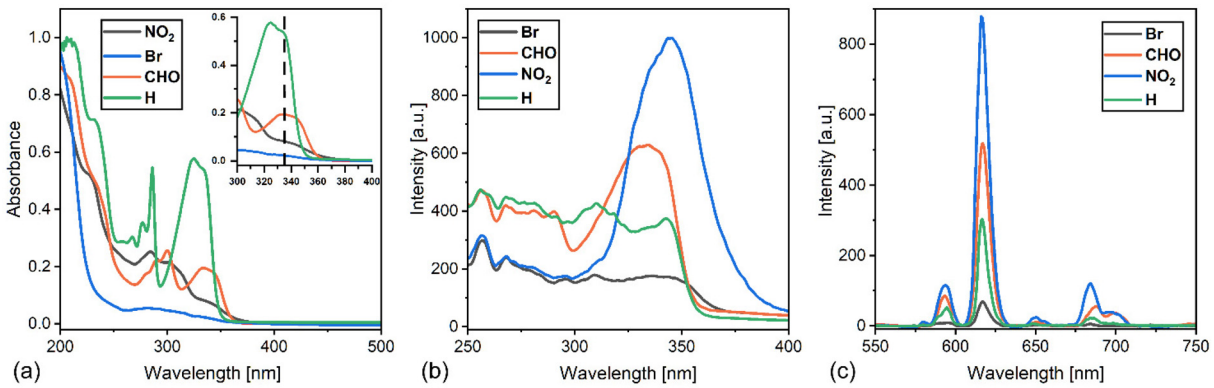

Fig. 3 Absorption (a), excitation (b), and emission (c) spectra of Eu-terpyR complexes [R = H (green), NO_2 (black), Br (blue), and CHO (red)] in acetonitrile at 298 K. λ_{exc} = 335 nm, λ_{em} = 617 nm, slit widths excitation = emission = 5 nm; scan rate = 250 nm min^{-1}; gain = 650 V; [complexes] = 0.10 mM.

Table 3 Energies (E) of singlet (^{1}S) and triplet (^{3}T) states of the ligands, distance (R_L) between acceptor (Ln(III)) and singlet (^{1}S) or triplet (^{3}T) states of the donor ligand, bandwidths (γ) of the peaks corresponding to ^{1}S and ^{3}T states of the ligands, emission lifetimes (τ) at 77 and 298 K, quantum yields of sensitized emission (ϕ_{Ln}^{L}), intrinsic quantum efficiency (ϕ_{Ln}^{Ln}) and sensitization efficiency (η_{sens}) for the Ln-terpyR (Ln = Eu, Tb, R = H, NO_2, CHO, Br) complexes

		terpy	terpyNO_2	terpyBr	terpyCHO
$E(^1S)^a$ [cm^{-1}]		27 950 ± 130 (lit. 26 178)[77]	27 900 ± 50	27 330 ± 200	28 000 ± 120
$E(^3T)^a$ [cm^{-1}]		22 200 ± 50 (lit. 20 041)[77]	22 860 ± 40	21 740 ± 40	21 880 ± 50
ΔE_{S-T} [cm^{-1}]		5750	5040	5590	6120
ΔE_{T-f^*}					
Eu		4970	5630	4510	4650
Tb		1700	2360	1240	1380
$R_L(^1S)$ [Å]		3.8071	3.8378	3.7071	3.8378
$R_L(^3T)$ [Å]		4.0296	4.1221	3.9202	3.9694
ϕ_{Ln}^{L} [%]					
Eu		9 ± 6 (lit. 1.3 (ref. 77))	26 ± 4	29 ± 6	29 ± 5
Tb		16 ± 6 (lit. 4.7 (ref. 77))	2 ± 2	22 ± 6	16 ± 4
ϕ_{Ln}^{Ln} [%]					
Eu		15 ± 1	53 ± 2	41 ± 3	46 ± 2
Tb		32.5 ± 0.3	20.3 ± 0.3	17.8 ± 0.3	29.3 ± 0.3
η_{sens} [%]					
Eu		60 ± 40	49 ± 8	71 ± 16	63 ± 11
Tb[c]		49 ± 18	10 ± 10	>90%[d]	55 ± 14
γ (^{1}S)[b] [cm^{-1}]		1120	490	1870	1560
γ (^{3}T)[b] [cm^{-1}]		770	400	890	750
τ [ms] (77 K)					
τ_1 (population)	Eu	0.30 ± 0.01 (70%)	0.40 ± 0.01 (61%)	0.75 ± 0.02 (44%)	0.25 ± 0.01 (69%)
τ_2 (population)		0.93 ± 0.01 (30%)	1.55 ± 0.01 (39%)	2.14 ± 0.02 (56%)	0.73 ± 0.01 (31%)
τ_1 (population)	Tb	0.42 ± 0.06 (15%)	0.24 ± 0.01 (30%)	0.79 ± 0.02 (63%)	0.53 ± 0.01 (21%)
τ_2 (population)		1.14 ± 0.03 (85%)	1.13 ± 0.01 (70%)	2.04 ± 0.01 (37%)	1.23 ± 0.01 (79%)
τ_{av} [ms] (77 K)					
Eu		0.49 ± 0.01	0.85 ± 0.01	1.53 ± 0.04	0.40 ± 0.01
Tb		1.03 ± 0.03	0.86 ± 0.01	1.25 ± 0.02	1.08 ± 0.01
τ [ms] (298 K)					
Eu		0.92 ± 0.01	1.49 ± 0.01	1.66 ± 0.01	1.68 ± 0.01
Tb		1.30 ± 0.01	0.81 ± 0.01	0.71 ± 0.01	1.17 ± 0.01
k_{rad} [s^{-1}]					
Eu		164.0 ± 9.2	358.0 ± 21.9	246.9 ± 5.3	272.6 ± 11.2
Tb[c]		250.0	250.0	250.0	250.0
k_{nrad} [s^{-1}]					
Eu		923.0 ± 9.2	313.1 ± 21.9	355.5 ± 5.3	322.6 ± 11.2
Tb		519.2	984.6	1158.5	604.7

[a] Indicated as the 0–0 transition after deconvolution of the fluorescence or phosphorescence spectra at 77 K (Fig. S57–S64).[89] [b] Determined as the full width at half maximum of the 0–0 transition. [c] Calculated assuming τ_{rad}(Tb(III)) = 4 ms.[45] [d] Calculations yielded an unrealistically high value of 124 ± 34, the more realistic lower limit value is presented in the table. Likely, this value is due to the assumed free ion τ_{rad} of 4 ms.

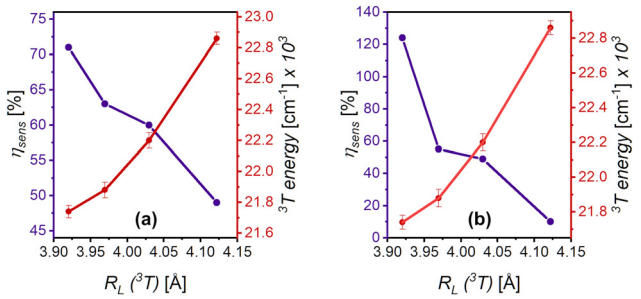

Fig. 4 Correlation between sensitization efficiency η_{sens}, the triplet state energy and the donor–acceptor distance $R_L(^3T)$ for the (a) Eu(III) complexes and (b) Tb(III) complexes.

narrow gaps observed for all systems should lead to substantial back-energy transfer for all except terpyNO_2, which has a gap of 2360 cm^{-1} (*vide infra*). A similar inverse correlation between η_{sens} and the triplet energies is seen for the Tb(III) complexes (Fig. 4b).

While the ^{3}T-f* gap[91] is frequently cited as the main criterion for efficient Ln(III) emission, it has been demonstrated that R_L, the distance between emissive state of the acceptor (Ln(III)) and the excited state of the donor (ligand) involved in the energy transfer to the Ln(III), also impacts the sensitization process.[92,93] Assuming that the energy transfer occurs mostly through the triplet, an increase in $R_L(^3T)$ is observed in the order terpyBr (3.9202 Å) < terpyCHO (3.9694 Å) < terpy (4.0296 Å) < terpyNO_2 (4.1221 Å). If the singlet is considered, the $R_L(^1S)$ are in the order terpyBr (3.7071 Å) < terpy (3.8071 Å) < terpyNO_2 (3.8378 Å) = terpyCHO (3.8378 Å). These values show a good correlation of the triplet energy, with η_{sens} and $R_L(^3T)$ for Eu(III) (Fig. 4a) and Tb(III) (Fig. 4b) complexes.

The room temperature emission lifetimes τ of the Eu(III) complexes (Table 3 and Fig. S49a–S56a), measured in acetonitrile, range from 0.92 to 1.68 ms; they could be fit to a single exponential, and are within the expected for this type of complexes. We attribute the longer lifetimes of the substituted

ligands to increased steric hindrance around the metal ion. Overall, the lifetimes for the Tb(III) complexes (Table 3 and Fig. S49–S56(a)) are in the range 0.71–1.30 ms. They are shorter than those of the Eu(III) complexes, except in the case of the terpy-based complexes. We attribute this difference to the slight size decrease of Tb(III) with respect to Eu(III); the structure of the terpyNO$_2$ complexes showed a slightly better fit of Eu(III) in the ligand cavity than Tb(III).[33] The lifetimes of the terpy-based complexes, 0.92 ms and 1.30 ms for the Eu(III) and Tb(III) complexes, are shorter than the reported values of 2.31 ms and 1.20 ms,[77] consistent with different ligand-to-metal ion stoichiometry of the complexes studied here (1 : 1), and by Mürner *et al.* (3 : 1).[77] At 77 K the emission decay (Fig. S49–S56b) is best fit with a double exponential for both ions, which is consistent with two conformations of the Ln(III)-complexes, as is discussed below.

The radiative (k_{rad}) and non-radiative (k_{nrad}) rate constants are similar for all substituted Eu-terpyR complexes. In contrast, the corresponding rate constants for the terpy complex are approximately 2 times lower for k_{rad} and about 2.5–3 times higher for k_{nrad}. This indicates that adding an EWG to the terpyridine *ortho*-position, regardless of its nature, leads to a simultaneous increase in luminescence emission rates and a decrease in non-radiative luminescence quenching. In the case of the Tb-complexes, the non-radiative processes dominate, particularly in the case of the highly electronegative groups –NO$_2$ and –Br.

Determination of the Judd–Ofelt parameters and energy transfer rates

To further unravel the complexity of the photophysical properties, we determined the experimental and theoretical Judd–Ofelt parameters Ω_2, Ω_4, and Ω_6 (Table 4). We used, as starting geometries for all complexes, the known X-ray single crystal structures of Eu-terpyNO$_2$ and Tb-terpyNO$_2$.[33] A good match between the calculated and experimental geometries (Fig. S65), and the calculated and experimental parameters Ω_2 and Ω_4 (Table 4) was obtained.

These spectral intensity parameters reflect numerous crystal field effects between the Ln(III) ion and its ligand environment; Ω_2 is very sensitive to distortions of the coordination sphere symmetry and changes in covalency of the Ln-ligand bonds, while Ω_4 and Ω_6 are more affected by bulk properties such as viscosity and rigidity.[5,94] For Eu(III) complexes, Ω_2 is strongly related to the hypersensitive $^5D_0 \rightarrow {}^7F_2$ emission peak.[94] The observed differences in Ω_2 correlate with the dis-

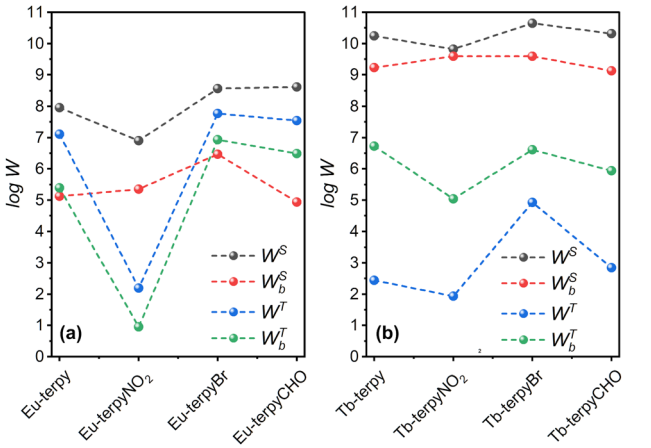

Fig. 5 Forward (W) and back energy transfer rates (W_b) related to ^{1}S–Ln (^{S}) (a) and ^{3}T–Ln (^{T}) transitions; (a) for Eu(III) complexes and (b) for Tb(III) complexes.

Table 4 Coordination polyhedra around the Eu(III) ion (yellow – Eu, red – O, blue – N, purple – Br), distortion of the experimental polyhedra (δ), and experimental and theoretical Judd–Ofelt parameters Ω_2, Ω_4, Ω_6, for the Eu(III) and Tb(III) complexes of terpyR (R = H, NO$_2$, Br, CHO)

Coordination number, polyhedron	9, monocapped square antiprism		10, bicapped square antiprism	
	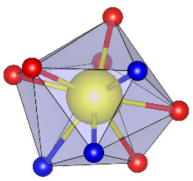	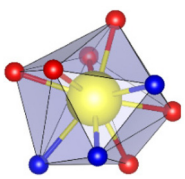	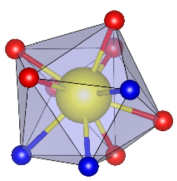	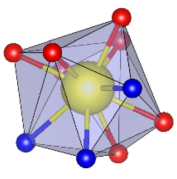
Complex	terpy	terpyBr	terpyNO$_2$	terpyCHO
δ	18.1	20.2	14.7	21.4
Eu-terpyR experimental parameters				
Ω_2 [×10^{-20} cm^2]	3.76 ± 0.25	8.57 ± 0.26	10.35 ± 0.50	12.83 ± 0.10
Ω_4 [×10^{-20} cm^2]	4.29 ± 0.19	2.65 ± 0.07	1.56 ± 0.28	4.50 ± 0.241
Eu-terpyR theoretical (RM1 Sparkle) parameters				
Ω_2 [×10^{-20} cm^2]	3.76	8.57	10.36	12.83
Ω_4 [×10^{-20} cm^2]	4.29	2.65	2.14	3.30
Ω_6 [×10^{-20} cm^2]	2.22	0.98	0.46	2.25
Tb-terpyR theoretical (RM1 Sparkle) parameters				
Ω_2 [×10^{-20} cm^2]	4.61	9.10	10.16	6.75
Ω_4 [×10^{-20} cm^2]	7.89	5.07	2.84	7.02
Ω_6 [×10^{-20} cm^2]	3.31	1.59	0.58	2.42

tortion parameter δ from the ideal polyhedron; the larger δ for a coordination polyhedron with the same coordination number, the larger the value of Ω_2. Lower values of Ω_4 and Ω_6 correspond to higher molecular rigidity. Based on this, the Eu(III) complexes with terpyBr and terpyCHO should have the longest emission lifetimes, which is observed experimentally.

The calculated forward W and back-energy W_b transfer rates involve transitions from the singlet ($^1S \rightarrow Ln$ (W^S)) (Fig. 5a) and triplet ($^3T \rightarrow Ln$ (W^T)) (Fig. 5b) states to the Ln(III) excited states and from those back to the ligand singlet ($Ln \rightarrow S$ (W_b^S)) and triplet ($Ln \rightarrow {}^3T$ (W_b^T)) states; their calculated numerical values, along with the Ln(III) energy levels participating in the transitions, are summarized in Tables S1–S2. W^S and corresponding W_b^S are higher in the case of Tb(III) complexes. Oppositely, W^T of Tb-complexes are considerably lower comparing to the Eu-terpyR, except Eu-terpyNO$_2$, for which W^T value is also very low. Thus, W_b^T are higher than W^T for all Tb-terpyR, whereas in the case of Eu-terpyR, W^T are higher than W_b^T.

Predominance of back-transfer processes in Tb(III) complexes correlates with the expectation that an efficient ligand-to-metal energy transfer with negligible back energy transfer is expected if the ligand's triplet state is >1850 cm^{-1} higher than the Tb(III) $^5D_4$ level (20 500 cm^{-1}).[91] This explains the higher values for Tb-terpyR W_b^T than W^T as the ligands' triplets energies lie in the range 21 740–22 860 cm^{-1}, close to the $^5D_4$ level. For Eu(III), experimental data indicates that ligands with a minimum triplet state energy of 19 800 cm^{-1} should easily transfer energy to the metal.[95–97]

Despite significant W_b^T, the sensitization of Tb still takes place, as evidenced by relatively large values of sensitization efficiency η_{sens} (Table 3). This includes an overestimated η_{sens} for Tb-terpyBr, likely caused by simplifying the estimate of this value with the assumption that τ_{rad} = 4 ms. Overall, the determined η_{sens} values correlate with the total rate of forward energy transfer W^{S+T} values, as shown in Fig. 6. An increase in total rate of energy transfer from ligand to Ln(III) increases η_{sens} (Fig. 6a and d). Conversely, W^{S+T} decreases with an increase in ^3T and $R_L(^3T)$ (Fig. 6b, c, e and f).[65] Moreover, as W^{S+T} depends on $1/R_L{}^4$ and $1/R_L$,[6] a modest increase of accep-

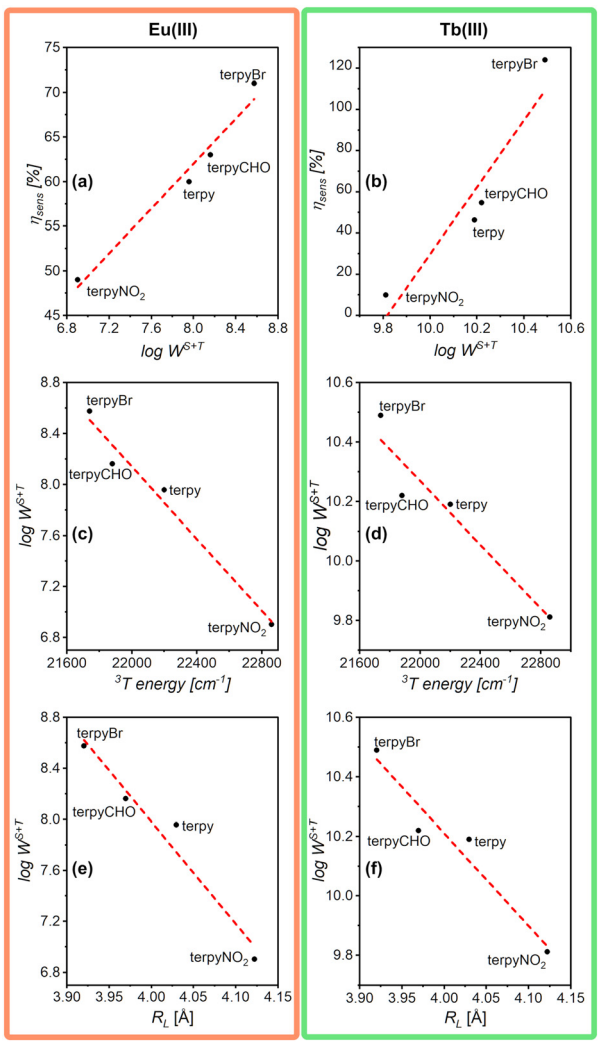

Fig. 6 Correlation between energy transfer rates and different parameters. Correlations related to the Eu(terpyR) complexes, between the logarithm of total forward transfer rates and sensitization efficiency (a), ligand triplet energy (b), donor–acceptor distance (c). Correlations related to the Tb(terpyR) complexes, between the logarithm of total forward transfer rates and sensitization efficiency (d), ligand triplet energy (e), and donor–acceptor distance (f).

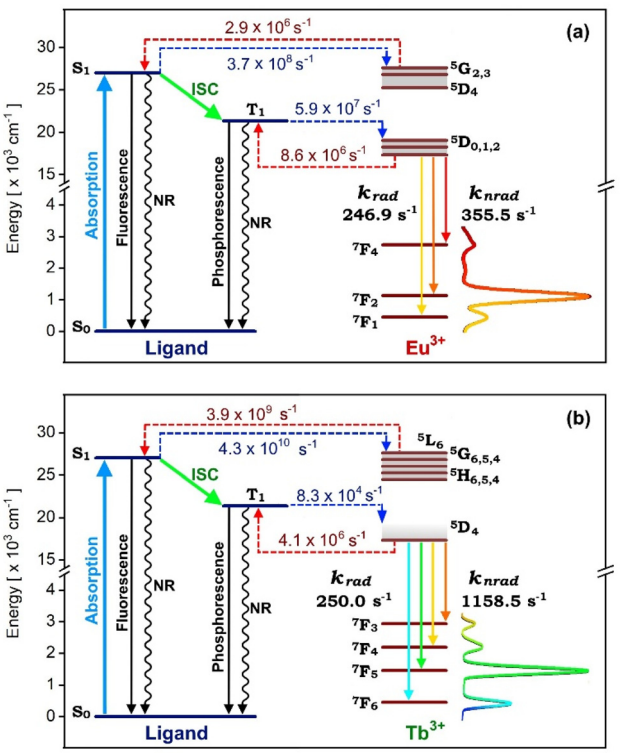

Fig. 7 Jabłoński diagram for Eu(terpyBr) (a) and Tb(terpyBr) (b)with energy transfer (red dashed lines and numbers) and back transfer (blue dashed lines and numbers) rates.

tor-donor distance leads to an increase in total W^{S+T} of almost two orders of magnitude from 7.9×10^6 to 3.7×10^8 s^{-1}.

A Jabłoński diagram for the Eu-terpyBr complex (Fig. 7), which exhibits the highest efficiency of sensitized emission ϕ_{Ln}^{L} = 29% (Table 3), summarizes that the rates of forward energy transfer are higher than those of back energy transfer. Jabłoński diagrams for the other Eu complexes are presented in the SI (Fig. S66–S68). A similar predominance of forward energy transfer is seen for the complexes Eu(terpyNO_2), and Eu (terpyCHO), which have efficiencies of sensitized emission close to 30%. The efficiency is smaller for Eu(terpy) (9%); while for this complex the forward rates are also higher, k_{nrad} is significantly larger than k_{rad} and thus also has the lowest intrinsic emission efficiency ϕ_{Ln}^{Ln} of 15%, while for the other Eu complexes this value is close to 50%, indicating a better vibrational shielding of the emissive state with the tetradentate ligands.

Tb(terpyBr) also displays the largest efficiency of sensitized emission ϕ_{Ln}^{L} = 22% (Table 3) and its Jabłoński diagram is shown in Fig. 7b. The analogous diagrams for the remaining Tb complexes are shown in Fig. S69–S71. For all four complexes, uniformly the rates of back-energy transfer to the ^{3}T state are higher than the forward energy transfer, consistent with the small ^{3}T-f* gap (Table 3). Moreover, large values of k_{nrad} lead to low values of ϕ_{Ln}^{L} for these complexes. The diagrams in Fig. 6 demonstrate that the triplet energy of the studied ligands decreases in the order NO_2 > CHO > Br. This trend inversely correlates with the forward energy transfer rates, which in turn directly correlate with the sensitization efficiency. Consequently, among the substituents considered, the sensitization efficiency of terpy ligands for Eu(III) and Tb (III) increases in the order NO_2 < H ≈ CHO < Br. However, this trend is not apparent from other properties, such as the complex stability constants (Table 1) or the distortions of the metal coordination sphere (Table 4). These observations highlight the importance of continuing the search for suitable synthetic modifications to design efficient Ln(III) sensitizers, as not only the energies of the singlet and triplet states influence energy transfer and sensitization efficiency, but also the donor–acceptor distances R_L and, as discussed below, the coordination environment around the Ln(III) ion.

Species leading to double-exponential emission lifetimes

While at room temperature the emission lifetimes fit a single exponential, at 77 K the emission lifetimes of all complexes could be fit with a double exponential. Chapman and co-workers[98] reported two conformations for terpy complexes of Ln(III), consistent with decomplexation and the rotation of one

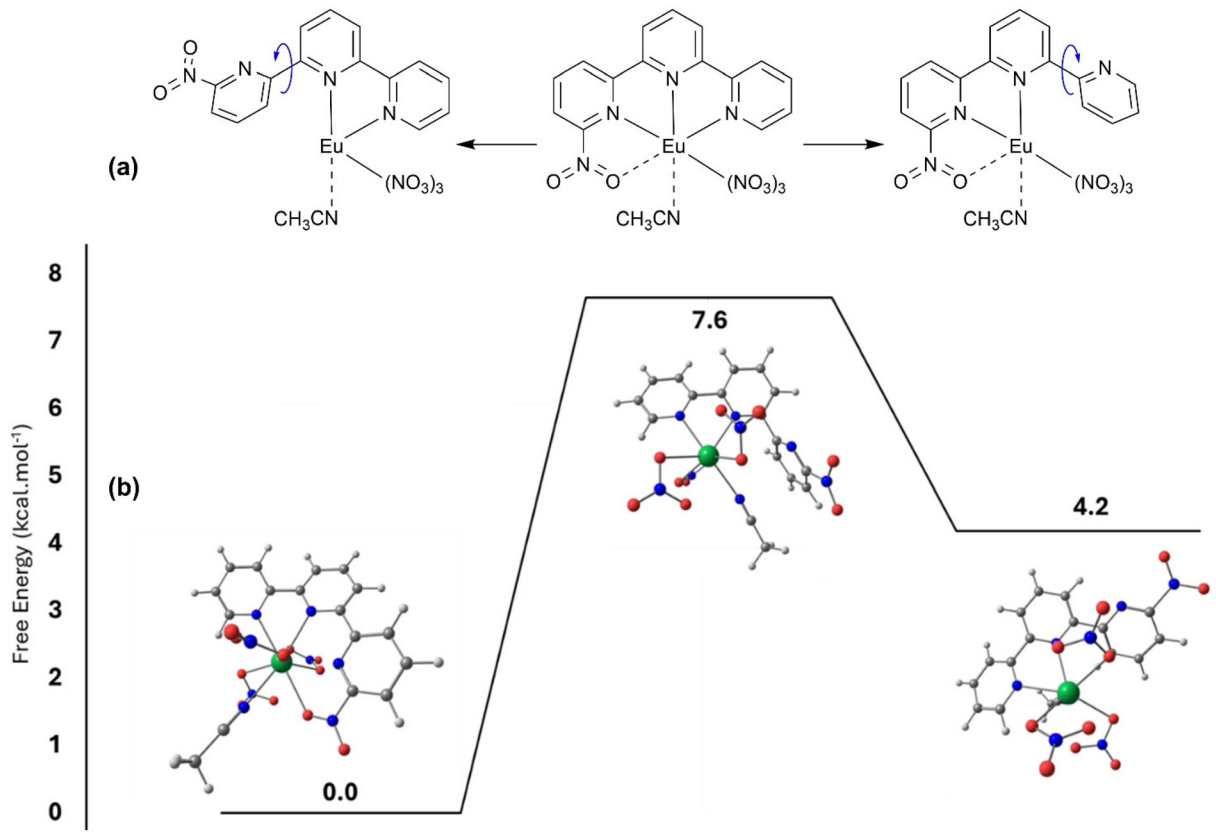

Fig. 8 (a) Three structures considered for the Eu(terpyNO_2) complex representing isomerization *via* decomplexation. (b) The free energy surface for the de-coordination of the pyridine nitrogen in the Eu(terpyNO_2)$(NO_3)_3$ complex. The structure on the left, right and middle are the geometries of the bound complex, unbound complex and the transition state structure respectively.

of the outside pyridine rings. These authors observed the coordination of terpyridine to Eu(III) in acetonitrile as a tridentate ligand in a *cis–cis–cis* conformation, and as a bidentate ligand with a *cis–cis–trans* conformation, with an acetonitrile molecule completing the coordination sphere. To assess the presence here of two species we calculated representatively, *via* a higher level of theory (relativistic Hamiltonian DKH2DFT), the isomerization for the Eu(terpyNO_2) complexes *via* the partial decomplexation of one of the pyridine rings followed by rotation of the pyridine ring away from the metal ion (Fig. 8a), either the unsubstituted ring, or the one containing the NO_2 group. From geometry optimization, we found that an acetonitrile solvent molecule coordinates to the Eu(III) ion.

Multiple coordination modes for the coordinated acetonitrile molecule were considered for the structure of the Eu(terpyNO_2) complex in the partially coordinated conformations, as there are multiple binding sites for the acetonitrile. The partially complexed isomer with the lowest computed relative free energy is 4.2 kcal mol^{-1} higher in energy than the completely coordinated complex. In this conformation, the NO_2-containing pyridine ring rotates, followed by a re-arrangement of the nitrate and acetonitrile molecules. Additionally, three other partially uncoordinated conformers with free energies at 5.9, 6.2, and 6.5 kcal mol^{-1} were found. Assuming the activation free energy of rotation for these different coordination modes are similar, the presence of mul-

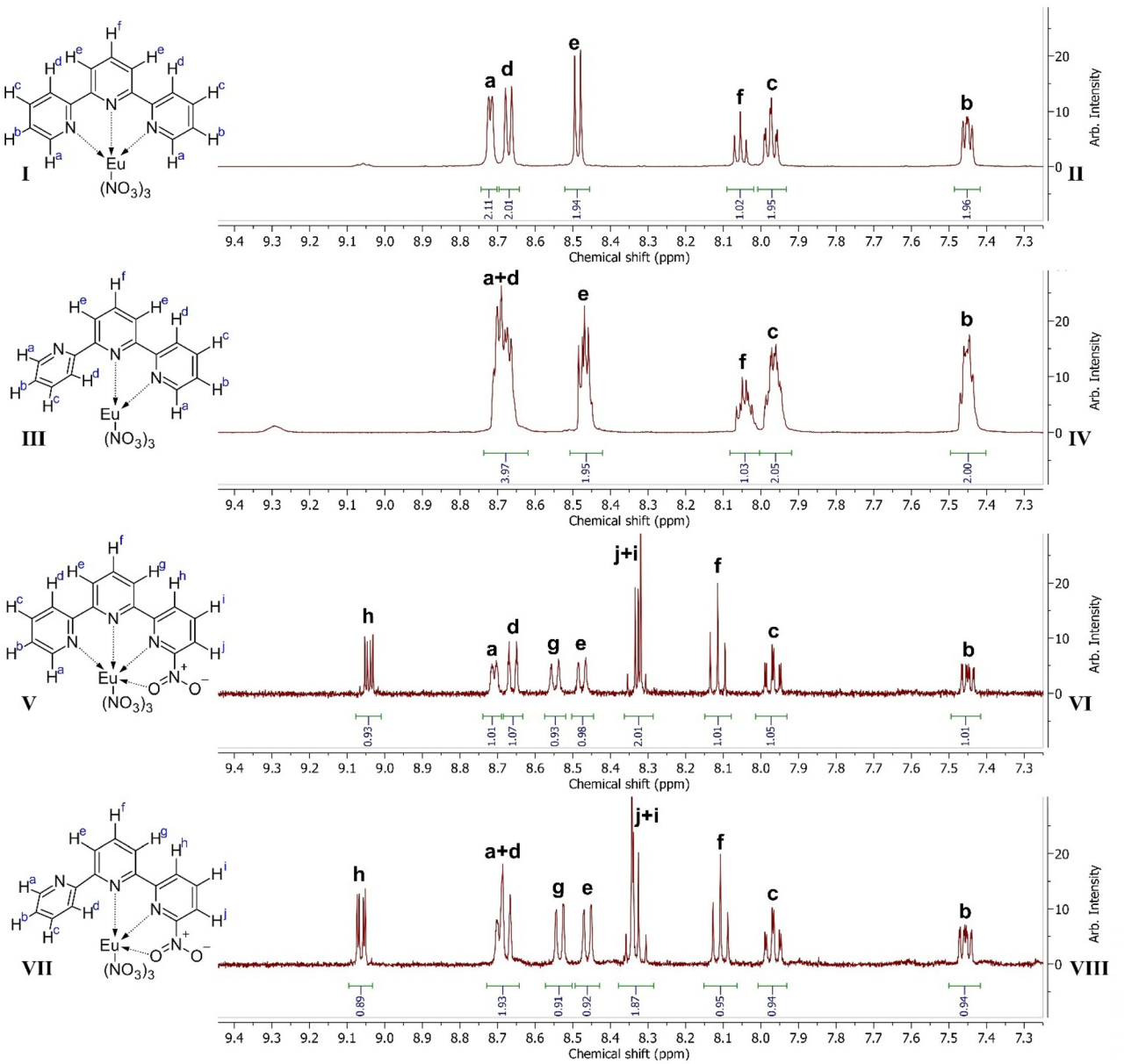

Fig. 9 ^{1}H-NMR spectra of Eu(terpy)$(NO_3)_3$ at (II) +24 °C and (IV) −30 °C and Eu(terpyNO_2)$(NO_3)_3$ at (VI) +24 °C and (VIII) −30 °C. Corresponding structural formulas (I, III, V, VII) are presented for clarity.

tiple different coordination mode shifts the equilibrium further towards the uncomplexed systems.

The activation free energy for the rotation of the pyridine ring was found to be 7.6 kcal mol^{-1} (Fig. 8b). Using the Arrhenius equation, and assuming a pre-exponential factor in the order of k_BT/h, the rate constants of forward and backward reactions at 77 K are in the order of 10^{-9} s^{-1} and 10^{3} s^{-1}, respectively. This is in contrast with the much higher rates of 10^{7} s^{-1} and 10^{10} s^{-1} for the forward and backward reactions at 300 K. This indicates that the interconversion between the fully coordinated complex and the partially uncoordinated complex isomers is orders of magnitude faster at 300 K than 77 K, which enables the presence of the two species at the lower temperature and is consistent with the double exponential decay.

Further experimental evidence for these two species was procured by ^{1}H-NMR spectroscopy. Comparison of spectra of Eu(terpy)$(NO_3)_3$ and Eu(terpyNO$_2$)$(NO_3)_3$ at room temperature (Fig. 9_I and 9_{II}), respectively) and at −30 °C (Fig. 9_{VII} and 9_{VIII}, respectively) show a splitting of peaks at the lower temperature, consistent with the formation of different structures. A noticeable downfield shift of the signal of the *meta*-hydrogen in the pyridine ring (denoted as H^d) was observed upon cooling. In the case of Eu(terpy)$(NO_3)_3$ the downfield shift of H^d is not easily observable due to overlapping signals. The signals corresponding to the H^d protons (8.67 ppm, ddt, J = 7.99, 1.16, 1.16 Hz) and the H^a protons (8.72 ppm, ddd, J = 4.83, 1.86, 0.98 Hz) are easily distinguishable (Fig. 9_{III}). Lowering the temperature causes the appearance of additional peaks in between these two, resulting in a multiplet at 8.69 ppm (Fig. 9_V).

For this complex, H^a (8.71 ppm, d, J = 4.79 Hz) and H^d (m, 8.66 ppm) can be easily distinguished at room temperature (Fig. 9_{IV}); however, they overlap at −30 °C (Fig. 9_{VI}). The shifts of other peaks are less prominent, consistent with the assumption that the distance between H^d and Eu(III) shortens upon rotation of the pyridine ring at lower temperature.

Conclusions

In this paper, we synthesized terpyridine ligands with different electron-withdrawing functional groups to study how the nature of these groups influences the formation of Eu and Tb complexes and the efficiency of sensitized emission in these complexes. We found that the higher stability constants of the complexes are obtained for the ligands with the highest pK_{a_2}, the second protonation constant of the terpyridine-based ligands. All complexes display Ln(III)-centred emission. Especially in the case of Eu(III), we found that the more distorted the structure of the polyhedron around the metal ion, the largest the Ω_2 Judd–Ofelt parameter, and such distortions were largest for the terpyBr and terpyCHO complexes; these also display the largest efficiency of sensitized emission for Eu (III). Lifetime measurements indicated the formation of two species at 77 K, which were explained, through DFT calculation and supported by ^{1}H-NMR measurements, by the formation of partially decomplexed structures, as had been previously observed for other terpy-based lanthanide complexes. Overall, these findings provide valuable design principles for designing terpyridine-based ligands to optimize the luminescence properties of lanthanide complexes. Ultimately, they highlight the complexity of tailoring ligand properties for sensitization of Ln (III)-centred emission; in addition to the energies of singlet and triplet states, coordination environment and donor–acceptor distances also play an important role.

Author contributions

Oksana Fizer: spectroscopic measurements, methodology writing – original draft. Sina Chiniforoush: computations, writing – original draft. Thomas J. Summers: computations. Mohammad Zafar Abbas: synthesis, writing – original draft. David C. Cantu: conceptualization, methodology, supervision. Ana de Bettencourt-Dias: conceptualization, methodology, writing – original draft & editing, supervision.

Conflicts of interest

There are no conflicts to declare.

Data availability

The data supporting this article have been included as part of the supplementary information (SI). Supplementary information: NMR and mass spectra, spectrophotometric titrations, absorption, excitation and emission spectra, emission decay curves, calculated energy transfer rates and calculated geometries. See DOI: https://doi.org/10.1039/d5dt02417j.

Acknowledgements

This work was financially supported by the U.S. Department of Energy, Office of Science, Office of Basic Energy Sciences, Created by the Competitive Research Incentive Program under grant number DE-SC0022178.

References

1 *Luminescence of Lanthanide Ions in Coordination Compounds and Nanomaterials*, ed. A. de Bettencourt-Dias, John Wiley and Sons, Hoboken, 2014.
2 C. M. Granadeiro, D. Julião, S. O. Ribeiro, L. Cunha-Silva and S. S. Balula, *Coord. Chem. Rev.*, 2023, **476**, 214914.
3 S. Zhang, W. Yin, Z. Yang, Y. Yang, Z. Li, S. Zhang, B. Zhang, F. Dong, J. Lv, B. Han, Z. Lei and H. Ma, *ACS Appl. Mater. Interfaces*, 2021, **13**(4), 5539–5550.

4 C. Chen, Y. Zhuang, X. Li, F. Lin, D. Peng, D. Tu, A. Xie and R. J. Xie, *Adv. Funct. Mater.*, 2021, **31**(25), 2101567.
5 V. X. Quang, P. Van Do, N. X. Ca, L. D. Thanh, V. P. Tuyen, P. M. Tan, V. X. Hoa and N. T. Hien, *J. Lumin.*, 2020, **221**, 117039.
6 V. V. Utochnikova, A. N. Aslandukov, A. A. Vashchenko, A. S. Goloveshkin, A. A. Alexandrov, R. Grzibovskis and J.-C. G. Bünzli, *Dalton Trans.*, 2021, **5**(37), 1286–12813.
7 K. Nehra, A. Dalal, A. Hooda, S. Bhagwan, R. K. Saini, B. Mari, S. Kumar and D. Singh, *J. Mol. Struct.*, 2022, **1249**, 131531.
8 A. Barkanov, A. Zakharova, T. Vlasova, E. Barkanova, A. Khomyakov, I. Avetissov, I. Taydakov, N. Datskevich, V. Goncharenko and R. Avetisov, *J. Mater. Sci.*, 2022, **57**(18), 8393–8405.
9 F. Zinna, M. Pasini, F. Galeotti, C. Botta, L. Di Bari and U. Giovanella, *Adv. Funct. Mater.*, 2017, **27**(1), 1603719.
10 A. de Bettencourt-Dias, *Dalton Trans.*, 2007, **22**, 2229–2241.
11 X. Qiu, J. Xu, M. Cardoso Dos Santos and N. Hildebrandt, *Acc. Chem. Res.*, 2022, **55**(4), 551–564.
12 L. Yu, Z. Gao, Q. Xu, X. Pan and Y. Xiao, *Biosens. Bioelectron.*, 2022, **210**, 114320–114320.
13 J. Wang, T. Sheng, X. Zhu, Q. Li, Y. Wu, J. Zhang, J. Liu and Y. Zhang, *Mater. Chem. Front.*, 2021, **5**(4), 1743–1177.
14 Y. Li, C. Chen, F. Liu and J. Liu, *Mikrochim. Acta*, 2022, **189**(3), 109–109.
15 H. Pham and L. W. Miller, in *Methods in Enzymology*, Academic Press, 2021, ch. 9.
16 H. Min, S. Wu, Z. Han, Z. Chen, T. Sun, W. Shi and P. Cheng, *Chem. – Eur. J.*, 2021, **27**(69), 17459–17464.
17 Y.-C. Chen and M.-L. Tong, *Chem. Sci.*, 2022, **13**(3), 8716–8726.
18 R. Marin, G. Brunet and M. Murugesu, *Angew. Chem., Int. Ed.*, 2021, **60**(4), 1728–1746.
19 Z. Zhu and J. Tang, *Natl. Sci. Rev.*, 2022, **9**(12), nwac194.
20 Tamanna and V. Mutreja, *Mater. Today: Proc.*, 2022, 2214–7853.
21 M. Patyal, K. Kaur, N. Bala, N. Gupta and A. K. Malik, *J. Trace Elem. Med. Biol.*, 2023, **80**, 127277–127277.
22 J. H. S. K. Monteiro, A. de Bettencourt-Dias, I. O. Mazali and F. A. Sigoli, *New J. Chem.*, 2015, **39**(3), 1883–1891.
23 A. de Bettencourt-Dias and J. S. K. Rossini, *Inorg. Chem.*, 2016, **55**, 9954–9963.
24 A. K. Duncan, C. N. McBride, T. G. R. Benjamin, M. P. Madsen, K. T. Bowers, A. de Bettencourt-Dias and E. J. Werner, *Polyhedron*, 2016, **114**, 451–458.
25 A. de Bettencourt-Dias, J. S. K. Rossini and J. A. Sobrinho, *Dalton Trans.*, 2020, **49**, 17699–17708.
26 J. H. S. K. Monteiro, N. R. Fetto, M. J. Tucker and A. de Bettencourt-Dias, *Inorg. Chem.*, 2020, **59**, 3193–3199.
27 P. S. Barber, A. de Bettencourt-Dias, K. R. Johnson and J. H. S. K. Monteiro, Ligand design in lanthanide complexes for luminescence, therapy, and sensing, in *Handbook on the Physics and Chemistry of Rare Earths*, ed. J.-C. G. Bünzli and S. Kauzlarich, Elsevier, 2024, vol. 65.
28 K.-X. Yu, J. G. C. Kragskow, Y.-S. Ding, Y.-Q. Zhai, D. Reta, N. F. Chilton and Y.-Z. Zheng, *Chem*, 2020, **6**(7), 1777–1793.
29 S. C. Corner, G. K. Gransbury, I. I. J. Vitorica-Yrezabal, G. F. S. Whitehead, N. F. Chilton and D. P. Mills, *Inorg. Chem.*, 2024, **63**(21), 9552–9561.
30 S. C. Corner, G. K. Gransbury, I. I. J. Vitorica-Yrezabal, G. F. S. Whitehead, N. F. Chilton and D. P. Mills, *Inorg. Chem.*, 2024, **63**(21), 9562–9571.
31 A. Ullah, J. S. Cerdá, J. J. Baldoví, S. A. Varganov, J. Aragó and A. Gaita-Ariño, In Silico, *J. Phys. Chem. Lett.*, 2019, **10**(24), 7678–7683.
32 J. Romanova, R. Lyapchev, M. Kolarski, M. Tsvetkov, D. Elenkova, B. Morgenstern and J. Zaharieva, *Molecules*, 2023, **28**(10), 4113.
33 A. de Bettencourt-Dias, S. Bauer, S. Viswanathan, B. C. Maull and A. M. Ako, *Dalton Trans.*, 2012, **41**, 11212–11218.
34 Y. Bretonnière, M. Mazzanti, J. Pécaut and M. M. Olmstead, *J. Am. Chem. Soc.*, 2002, **124**(31), 9012–9013.
35 X.-Y. Chen, Y. Bretonnière, J. Pécaut, D. Imbert, J.-C. Bünzli and M. Mazzanti, *Inorg. Chem.*, 2007, **46**(3), 625–637.
36 Y. Sakai, S. Mizuta, A. Kumagai, M. S. O. Tagod, H. Senju, T. Nakamura, C. T. Morita and Y. Tanaka, Cells, *ChemMedChem*, 2017, **12**(23), 2006–2013.
37 P. J. Vallett and N. H. Damrauer, *J. Phys. Chem.*, 2011, **115**(14), 3122–3132.
38 A. de Bettencourt-Dias, S. Bauer, S. Viswanathan, B. C. Maull and A. M. Ako, *Dalton Trans.*, 2012, **41**(36), 11212–11218.
39 T. J. Summers, J. A. Sobrinho, A. de Bettencourt-Dias, S. D. Kelly, J. L. Fulton and D. C. Cantu, *Inorg. Chem.*, 2023, **62**(13), 5207–5218.
40 J. A. Mattocks, J. L. Tirsch and J. A. Cotruvo Jr, *Methods Enzymol.*, 2021, **651**, 23–61.
41 A.-S. Chauvin, F. Gumy, D. Imbert and J.-C. G. Bünzli, *Spectrosc. Lett.*, 2004, **37**(5), 517–532.
42 S. I. Klink, G. A. Hebbink, L. Grave, P. G. B. Alink, F. C. J. M. van Veggel and M. H. V. Werts, *J. Phys. Chem. A*, 2002, **106**(15), 3681–3689.
43 A. Aebischer, F. Gumy, J. C. G. Bünzli, A. Aebischer and F. Gumy, *Phys. Chem. Chem. Phys.*, 2009, **11**(9), 1346–1353.
44 M. H. V. Werts, R. T. F. Jukes and J. W. Verhoeven, *Phys. Chem. Chem. Phys.*, 2002, **4**, 1542–1548.
45 S. I. Klink, L. Grave, D. N. Reinhoudt, F. C. J. M. van Veggel, M. H. V. Werts, F. A. J. Geurts and J. W. Hofstraat, *J. Phys. Chem. A*, 2000, **104**(23), 5457–5468.
46 Y. D. M. Champouret, R. K. Chaggar, I. Dadhiwala, J. Fawcett and G. A. Solan, *Tetrahedron*, 2006, **62**, 79–89.
47 C. J. Mallon, M. Hassani, M. Fizer, S. A. Varganov, A. de Bettencourt-Dias and M. J. Tucker, *Phys. Chem. A*, 2025, **129**(20), 4374–4383.
48 Y. Toya, K. Hayasaka and H. Nakazawa, *Organometallics*, 2017, **36**(9), 1727–1735.
49 Y. D. M. Champouret, R. K. Chaggar, I. Dadhiwala, J. Fawcett and G. A. Solan, *Tetrahedron*, 2006, **62**(1), 79–89.

50 O. Kuleshova, S. Asako and L. Ilies, *ACS Catal.*, 2021, **11**(10), 5968–5973.
51 Y. Zhao and D. G. Truhlar, *Theor. Chem. Acc.*, 2008, **119**(5–6), 525–525.
52 X. Cao and M. Dolg, *J. Mol. Struct.*, 2002, **581**(1), 139–147.
53 T. H. Dunning, *J. Chem. Phys.*, 1989, **90**(2), 1007–1023.
54 D. Aravena, F. Neese and D. A. Pantazis, *J. Chem. Theory Comput.*, 2016, **12**(3), 1148–1156.
55 A. Z. de Oliveira, I. B. Ferreira, C. T. Campos, F. E. Jorge and P. A. Fantin, *Mol. Model.*, 2019, **25**(2), 38–39.
56 F. E. Jorge, L. S. C. Martins and M. L. Franco, *Chem. Phys. Lett.*, 2016, **643**, 84–88.
57 M. Reiher, *WIREs: Comput Mol Sci*, 2012, **2**(1), 139–149.
58 M. Cossi, N. Rega, G. Scalmani and V. Barone, *J. Comput. Chem.*, 2003, **24**(6), 669–681.
59 K. Mansouri, N. F. Cariello, A. Korotcov, V. Tkachenko, C. M. Grulke, C. S. Sprankle, D. Allen, W. M. Casey, N. C. Kleinstreuer and A. J. Williams, *J. Cheminf.*, 2019, **11**(1), 60–20.
60 J. D. L. Dutra, T. D. Bispo and R. O. Freire, *J. Comput. Chem.*, 2014, **35**(10), 772–775.
61 M. A. M. Filho, J. D. L. Dutra, G. B. Rocha, R. O. Freire and A. M. Simas, *RSC Adv.*, 2013, **3**(37), 16747–16755.
62 A. B. Ganaie and K. Iftikhar, *ACS Omega*, 2021, **6**(33), 21207–21226.
63 J. J. P. Stewart, *Stewart Computational Chemistry*, Colorado Springs, CO, USA, 2016. https://openmopac.net/.
64 F. Neese, Software update: The ORCA program system—Version 5.0, *Wiley Interdiscip. Rev.:Comput. Mol. Sci.*, 2022, **12**(5), e1606.
65 R. T. Moura Jr, A. N. Carneiro Neto, E. C. Aguiar, C. V. Santos-Jr, E. M. de Lima, W. M. Faustino, E. E. S. Teotonio, H. F. Brito, M. C. F. C. Felinto, R. A. S. Ferreira, L. D. Carlos, R. L. Longo and O. L. Malta, *Opt. Mater.:X*, 2021, **11**, 100080.
66 L. Link and R. Niewa, *J. Appl. Crystallogr.*, 2023, **56**(6), 1855–1864.
67 C. Hübler, *Chem.:Methods*, 2022, **2**(7), e202200006.
68 I. Hemmila, V. M. Mukkala, M. Latva and P. Kiilholma, *J. Biochem. Biophys. Methods*, 1993, **26**(4), 283–290.
69 M. Latva, H. Takalo, V.-M. Mukkala and J. Kankare, *Inorg. Chim. Acta*, 1998, **267**(1), 63–72.
70 G. Muller, J.-C. G. Bünzli, J. P. Riehl, D. Suhr, A. von Zelewsky and H. Muerner, *Chem. Commun.*, 2002, **14**, 1522–1523.
71 Y. Bretonniere, M. Mazzanti, J. Pecaut and M. M. Olmstead, *J. Am. Chem. Soc.*, 2002, **124**(31), 9012–9013.
72 L. J. Charbonnière, S. Mameri, D. Flot, F. Waltz, C. Zandanel and R. F. Ziessel, *Dalton Trans.*, 2007, **22**, 2245–2253.
73 X. Y. Chen, Y. Bretonnière, J. Pecaut, D. Imbert, J. C. G. Bünzli and M. Mazzanti, *Inorg. Chem.*, 2007, **46**(3), 625–637.
74 S. A. Cotton, O. E. Noy, F. Liesener and P. R. Raithby, *Inorg. Chim. Acta*, 2003, **344**, 37–42.
75 A. Escande, L. Guénée, K.-L. Buchwalder and C. Piguet, *Inorg. Chem.*, 2009, **48**(3), 1132–1147.
76 C. Mallet, R. P. Thummel and C. Hery, *Inorg. Chim. Acta*, 1993, **210**, 223–231.
77 H.-R. Mürner, E. Chassat, R. P. Thummel and J.-C. G. Bünzli, *Dalton Trans.*, 2000, 2809–2816.
78 B. Song, G. Wang, M. Tan and J. Yuan, *J. Am. Chem. Soc.*, 2006, **128**(41), 13442–13450.
79 K. Mizuno, M. Kurihara, S. Takagi and H. Nishihara, *Chem. Lett.*, 2003, **32**(9), 788–789.
80 M. Ichikawa, T. Yamamoto, H.-G. Jeon, K. Kase, S. Hayashi, M. Nagaoka and N. Yokoyama, *J. Mater. Chem.*, 2012, **22**(14), 6765–6773.
81 A. R. Stefankiewicz, M. Wałęsa-Chorab, J. Harrowfield, M. Kubicki, Z. Hnatejko, M. Korabik and V. Patroniak, *Dalton Trans.*, 2013, **42**(5), 1743–1751.
82 Q.-R. Wu, J.-J. Wang, H.-M. Hu, Y.-Q. Shangguan, F. Fu, M.-L. Yang, F.-X. Dong and G.-L. Xue, *Inorg. Chem. Commun.*, 2011, **14**(3), 484–488.
83 J. K. Molloy, Z. Pillai, J. Sakamoto, P. Ceroni and G. Bergamini, *Asian J. Org. Chem.*, 2015, **4**(3), 251–255.
84 X. Yu, Y. Hu, C. Guo, Z. Chen, H. Wang and X. Li, *Supramol. Mater.*, 2022, **1**, 100017.
85 D. A. Durham, G. H. Frost and F. A. Hart, *J. Inorg. Nucl. Chem.*, 1969, **31**(3), 833–838.
86 R. D. Shannon, *Acta Crystallogr., Sect. A*, 1976, **32**, 751–767.
87 E. Farkas, É.A Enyedy, G. Micera and E. Garribba, *Polyhedron*, 2000, **19**(14), 1727–1736.
88 B. P. Dailey and J. N. Shoolery, *J. Am. Chem. Soc.*, 1955, **77**(15), 3977–3981.
89 G. A. Crosby, R. E. Whan and R. M. Alire, *J. Chem. Phys.*, 1961, **34**(3), 743–748.
90 F. J. Steemers, W. Verboom, D. N. Reinhoudt, E. B. van der Tol and J. W. Verhoeven, *J. Am. Chem. Soc.*, 1995, **117**(37), 9408–9414.
91 M. Latva, H. Takalo, V.-M. Mukkala, C. Matachescu, J. C. Rodriguez-Ubis and J. Kankare, *J. Lumin.*, 1997, **75**, 149–169.
92 J. H. Monteiro, A. de Bettencourt-Dias and F. A. Sigoli, *Inorg. Chem.*, 2017, **56**(2), 709–712.
93 A. N. Carneiro Neto, L. S. D. Carlos, O. L. Malta, M. Sanadar, A. Melchior, E. Kraka, S. Ruggieri, M. Bettinelli and F. Piccinelli, *Inorg. Chem.*, 2022, **61**(41), 16333–16346.
94 C. K. Jørgensen and R. Reisfeld, *J. Less-Common Met.*, 1983, **93**(1), 107–112.
95 X. Zhai, P. Feng, N. Song, G. Zhao, Q. Liu, L. Liu, M. Tang and Y. Tang, *Inorg. Chem. Front.*, 2022, **9**(7), 146–1415.
96 X. Mi, D. Sheng, Y. E. Yu, Y. Wang, L. Zhao, J. Lu, Y. Li, D. Li, J. Dou, J. Duan and S. Wang, *ACS Appl. Mater. Interfaces*, 2019, **11**(8), 7914–7926.
97 C. H. Hossack, R. J. Butcher, C. L. Cahill and C. Besson, *Inorg. Chem.*, 2021, **60**(20), 15724–15743.
98 R. D. Chapman, R. T. Loda, J. P. Riehl and R. W. Schwartz, *Inorg. Chem.*, 1984, **23**, 1652–1657.